Design and analysis of a tensegrity mechanism for a bio-inspired robot

Swaminath Venkateswaran, Matthieu Furet, Damien Chablat, Philippe Wenger

Design and analysis of a tensegrity mechanism for a bio-inspired robot

Swaminath Venkateswaran[1,2], Matthieu Furer[1,2], Damien Chablat[2,3], Philippe Wenger[2,3]
[1]Ecole Centrale de Nantes, Nantes, 44321 France
[2]Laboratoire des Sciences du Numérique de Nantes (LS2N), UMR CNRS 6004, Nantes, 44300, France
[3]Centre National de la Recherche Scientifique (CNRS), Nantes, 44321, France
Emails: {swaminath.venkateswaran, matthieu.furet, damien.chablat, philippe.wenger}@ls2n.fr

July 22, 2019

Abstract

Piping inspection robots are of greater interests in industries such as nuclear, chemical and sewage. The design of such robots is highly challenging owing to factors such as locomotion inside pipes with varying diameters, cable management,and complex pipe bends (or) junctions. A rigid bio-inspired caterpillar type piping inspection robot was developed at LS2N, France. By introducing tensegrity mechanisms and four-bar wheel mechanisms, the design of this robot is modified into a reconfigurable system. The tensegrity mechanism employs a passive universal joint with three tension springs and three cables for actuation. The positioning of the end effector with respect to the base of the mechanism plays an important role in determining the maximum tilt angle (or) bending limit of the system. By workspace analysis of three case studies, the best solution is chosen which generates the maximum tilt. A static force analysis is then performed on the mechanism to determine its stability under the influences of preload. By the modification of design parameters, stable configurations are determined followed by which cable actuation of mechanism is analyzed for estimating applied forces.

INTRODUCTION

Piping inspection robots have a major attraction in the scientific research community. They could be used in applications for industries such as nuclear, chemical and sewage where it is usually cumbersome for a human being to perform the desired inspection activity. Some of the main design criteria that have to be kept in mind for these robots are their locomotion principle, contact system with pipeline walls, cable management and articulation units for facilitating the robot to pass through curvilinear pipe profiles. During locomotion, at any instant the diameter of pipeline is unknown and it is essential for the robot to have deployable or retracting modules that can work in such unknown diameter ranges. Several researches have been proposed and developed in this area of robotics for varying diameter pipelines. For example, Ankit et al. [1] proposed a screw type robot that is capable of working inside 127-152 mm diameter pipes. Zhang et al.[2] developed an inchworm-type robot that can adapt itself to varying pipe diameters. Kwon et al. [3] developed an inspection robot that employs a caterpillar module with four bar linkages to work inside 100 mm diameter pipes having bends and junctions. However, the main challenge lies in the development of a robot for pipelines having diameters less than 100 mm. As the diameter of the pipeline reduces, careful attention has to be given to the selection of mechanical systems that can adapt itself to make tight contacts with the walls. A bio-inspired caterpillar type piping inspection robot was developed by Henry et al [4]. This robot is capable of working inside 50-94 mm diameter pipelines. However, the robot is a rigid prototype which limits its application inside pipelines having bends (or) junctions. Also, the velocity of the motors used in the robot is very low and the cable management issues were not addressed.

In this article, we focus extensively on the modification of the caterpillar type robot into a reconfigurable system. A tensegrity type mechanism that employs a passive universal joint with three tension loaded springs is proposed to be introduced in the robot. Prior to the design and analysis of this articulation unit, some key design criteria is addressed which is essential for a robot to pass through pipe bends or junctions. With the help of Maple, the vector equations are generated for the tensegrity mechanism. The tilting of the mechanism is first studied to understand its posture under the influence of a cable force. For the estimation of the maximum bend (or) tilt angles, three possible case studies are generated for the mechanism. By workspace analysis, the best configuration is chosen which will facilitate the robot to bend upto maximum angle possible when passing through a pipe bend or junction. A static force analysis is performed on the mechanism in order to determine its stability with zero applied forces and with a preload. With the stable configurations determined, the necessary forces that have to be applied to the mechanism for working through curved pipe profiles are analyzed.

The outline of the article is as follows. The key design factors for a robot to pass through pipe bends and the architecture of modified robot design is discussed. Followed by that the design of the tensegrity mechanism is

presented. Analysis of the mechanism is then done for determining the ideal base orientation and then a workspace analysis is performed for three case studies of the system. The subsequent section deals with the static force analysis and estimation of forces to be applied to the mechanism. The article then ends with conclusions and future works.

ARCHITECTURE OF THE ROBOT

A bio-inspired robot for the inspection of pipelines has been designed and developed at LS2N, France by Henry et al. and Chablat et al [4, 5]. This robot accomplishes the locomotion of a caterpillar in six steps for moving inside pipes. Using leg mechanisms and EC-Motors, the prototype was developed and tested. However, this robot is a rigid model and it cannot be used for pipelines having bends or junctions. By the addition of suitable articulation units, the design of the robot can be modified into a reconfigurable mechanism. Before the design of articulation unit, some key issues have to be addressed for a robot that has to pass through pipe bends or junctions which are: the passive compliance, the active compliance,and tilt angle limits. Passive compliance could be imagined for a robot that has to pass through a pipe bend at 90 degrees or less. For addressing this compliance, the articulation unit need not be necessarily active. An example would be the robot of Zhang et al. [2] which uses a passive flexible helical axle to pass through 90-degree bends. In the case of active compliance, it is necessary for the articulation unit to be active. For a robot to pass through a T-junction or an elbow, the articulation unit needs to be actuated in order to decide the best path to be followed as well as maintain contact with pipeline walls. The third important factor is the tilt or bending angle limit of the articulation unit. As a robot passes through a pipe bend of 90 degrees or less, it is necessary for the articulation unit to bend up to a certain angle. The tilt angle range is generally defined by a cone of $\pm\, x$ degrees. The three factors are represented in Fig. 1.

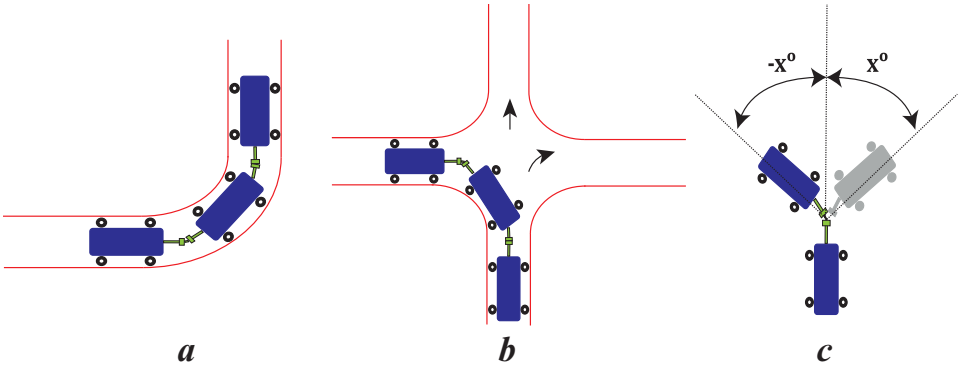

Figure 1: Representation of the passive (a) & active compliance's (b) and tilt angle range (c)

Modified design of the robot

The existing bio-inspired robot is made reconfigurable by introducing articulation units and four-bar wheel mechanisms. The outline of the modified bio-inspired robot is shown in Fig. 2.

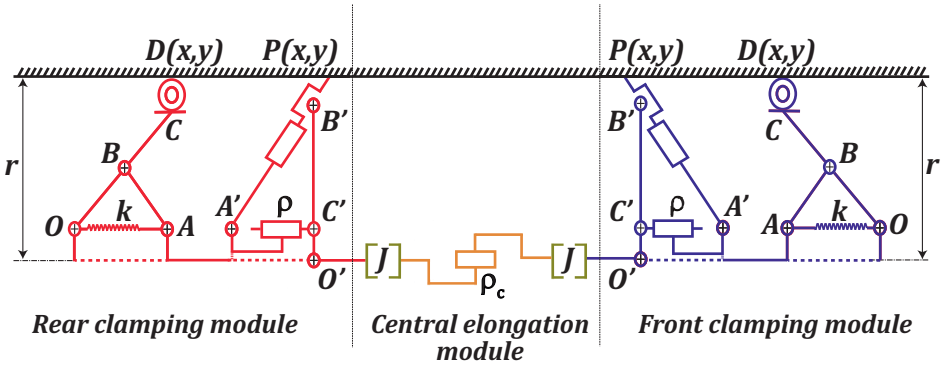

Figure 2: Outline of the modified bio-inspired piping inspection robot inside a pipeline of radius r

The caterpillar module represented by $O'C'A'B'$ is retained in the modified design for having contact with pipeline wall during static and dynamic phases. $OABCD$ represents a spring-loaded four-ball wheel mechanism. They ensure contact with the pipeline wall at all instances of locomotion. Also, this mechanism can assist the robot to smoothly

enter and exit pipe bends or junctions. The parameters ρ and ρ_c represents the clamping and central system actuation units. The joint J represents the new articulation unit that will be introduced in the robot. In the existing prototype, the front and central modules were bolted together but in the proposed design all the modules are being made independent. As the robot moves through a pipe bend, it resembles an "Elephant Trunk". By ensuring tight contact with pipeline walls using the caterpillar module, the force is transmitted from the front to rear end of the robot which will allow the robot to pass through or overcome the pipe bend.

Design of a tensegrity mechanism

In this article, we focus on the design of a suitable articulation unit that could address the issues of compliances and tilt limits discussed in the previous section. A tensegrity type mechanism is proposed to be introduced between the motor modules which can facilitate the robot to pass through 90-degree bends or junctions by bending up to a certain angle. In the existing design of the robot, the motor units were coupled rigidly. Between each unit, a universal joint and three tension springs are introduced. The universal joint remains passive and the issue of passive compliance could be addressed by this joint and springs for a 90-degree pipe bend. For active compliance, cables will be introduced that can pass through the springs. From a central control unit, the cables can be actuated and the robot can be made to move or bend along a fixed direction while encountering a junction. The proposed tensegrity mechanism is represented in Fig. 3.

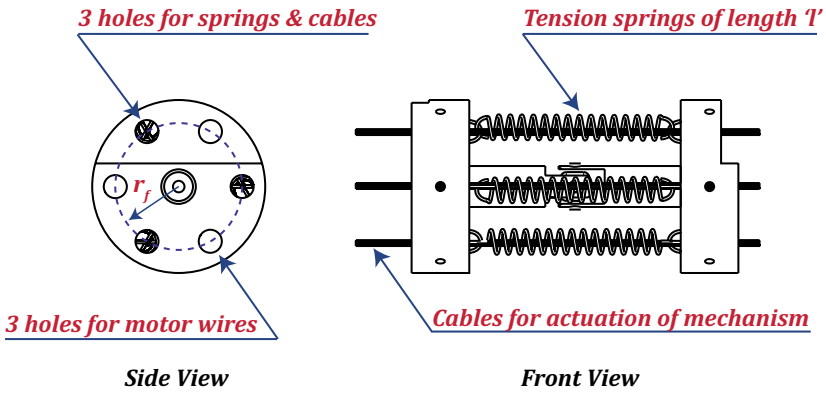

Figure 3: The proposed tensegrity mechanism with universal joint, springs and cables

The tensegrity system resembles the robot analyzed by Yigit et al. [6] but in the proposed design three tensions springs are used over a single compression spring of [6]. The flanges used for spring mounting is carried over from the existing prototype. The three springs are mounted at an angle of 120 degrees between each other. Three tension springs are used because they ensure stability of the system as well as the bending limit of the universal joint is controlled when the robot works through 3D pipe profiles. Three cables for actuation of the system passes through the springs. The other three holes on the flange can be used for routing the wires coming out from the motors used in the caterpillar module. The springs are mounted at radius r_f from the central axis of the flange. Using CATIA software, a 3D model of the tensegrity system is created by referencing dimensions from standard parts available at LS2N. The flanges are produced by 3D printing. With a standard universal coupling and three tension springs of stiffness $k = 0.2$ N/mm, the prototype is realized and it is depicted in Fig. 4.

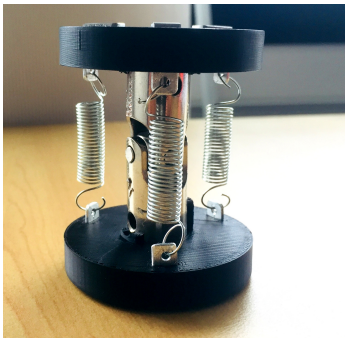

Figure 4: A prototype of the tensegrity mechanism created using 3D printing and standard parts without cables

In order to determine the maximum tilt limits, the radius r_f and the distance l between the flanges have to be considered for analysis which will be exploited in the next section.

ANALYSIS OF THE TENSEGRITY MECHANISM

In order to identify the constraints of the tensegrity mechanism, the equations of the system have to be derived. The complete tensegrity mechanism represented in Fig. 3 could be correlated to a parallel manipulator of type 3-SPS-U [7]. The 3D and 2D views of the correlation are represented in Fig. 5.

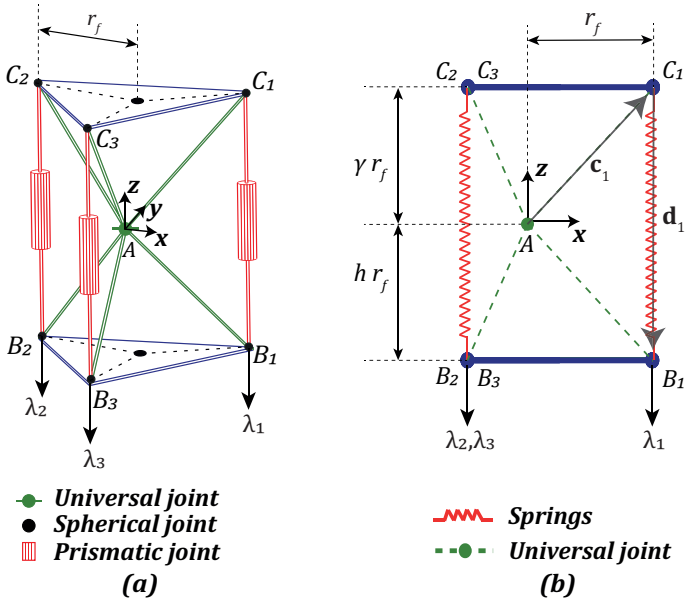

Figure 5: 3D (left) and 2D (right) representations of the tensegrity mechanism to a 3-SPS-U parallel manipulator (home-pose)

Figure 5 also represents the default or home-pose of the mechanism with no bending or forces. The points B_1, B_2 and B_3 represents the base of mechanism. The central point A is the origin of the universal joint. The end-effector positions are given by C_1, C_2 and C_3. The vector coordinates for B_i is given by:

$$\mathbf{b}_i = \mathbf{R}_z(\theta)\ \mathbf{n}_i, \qquad \text{with} \quad i = 1, 2, 3 \tag{1}$$

$$\text{where} \quad \mathbf{R}_z(\theta) = \begin{bmatrix} c_\theta & -s_\theta & 0 \\ s_\theta & c_\theta & 0 \\ 0 & 0 & 1 \end{bmatrix} \quad \& \quad \mathbf{n}_i = \begin{bmatrix} r_f \cos\left(\frac{2\pi(i-1)}{3}\right) \\ r_f \sin\left(\frac{2\pi(i-1)}{3}\right) \\ -r_f h \end{bmatrix}$$

where $\mathbf{n}_i$ are the coordinates of B_i in the local reference frame. The rotation matrix $\mathbf{R}_z$ with respect to θ is used for determining the rotation/orientation of mechanism about z-axis inside the pipe. The parameter h is a constant and it can assume values greater than zero. In order to estimate the positions of end-effector C_i, the theory of tilt & torsion (T&T) is employed. The T&T theory is employed mainly for parallel manipulators where the robot platform is mobile and asymmetric [8]. Since the universal joint is passive, the tilt and azimuth angles would be sufficient to calculate the positions of end-effectors as there is no torsion. The tilt and azimuth angles of the tensegrity mechanism are represented in Fig. 6.

β represents the azimuth angle between the x-axis and face of the z-axis. Rotation about M causes a shift of the axis xyz to $x^*y^*z^*$. The angle between z and z^* represents the tilt, α. The rotation matrix $\mathbf{R}$ for the tilt and azimuth angles is given by the equation:

$$\mathbf{R} = \mathbf{R}_z(\beta)\mathbf{R}_x(\alpha)\mathbf{R}_z(-\beta) \tag{2}$$

$$\mathbf{R} = \begin{bmatrix} (c_\alpha + c_\beta^2(1-c_\alpha) & -c_\beta s_\beta(c_\alpha - 1) & s_\beta s_\alpha \\ -c_\beta s_\beta(c_\alpha - 1) & 1 + (c_\alpha - 1)c_\beta^2 & -c_\beta s_\alpha \\ -s_\beta s_\alpha & c_\beta s_\alpha & c_\alpha \end{bmatrix} \tag{3}$$

In order to obtain the position of end-effector, Eqn. (3) is multiplied by the vector coordinates of positions C_i and the equation is given by:

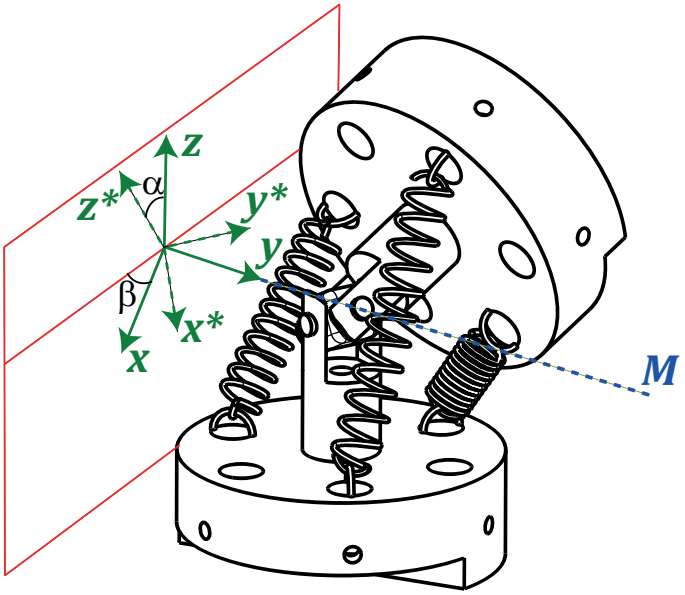

Figure 6: Representation of Tilt (α) and Azimuth (β) angles on the tensegrity mechanism

$$\mathbf{c}_i = \mathbf{R}_z(\theta)\ \mathbf{R}\ \mathbf{o}_i, \qquad \text{with} \quad i = 1, 2, 3 \tag{4}$$

$$\text{where} \quad \mathbf{o}_i = \begin{bmatrix} r_f \cos\left(\frac{2\pi(i-1)}{3}\right) \\ r_f \sin\left(\frac{2\pi(i-1)}{3}\right) \\ r_f \gamma \end{bmatrix}$$

where $\mathbf{o}_i$ are the coordinates of C_i in the local reference frame of the mobile platform. The parameter γ is a scalar value that determines the position of end-effector from the origin A. The workspace analysis for various values of γ will be analyzed in the upcoming section. The length of the mechanism l_i which provides the solution for the inverse kinematic problem can be solved and it is given by the equations below:

$$\mathbf{b}_i = [b_{ix}, b_{iy}, b_{iz}]^T, \mathbf{c}_i = [c_{ix}, c_{iy}, c_{iz}]^T \quad \text{with } i = 1, 2, 3$$

$$l_i = \sqrt{(b_{ix} - c_{ix})^2 + (b_{iy} - c_{iy})^2 + (b_{iz} - c_{iz})^2} \tag{5}$$

Tilting direction of the mechanism

For an applied force, the tensegrity mechanism has to tilt along the direction of force. The position of β is identified where the mechanism tilts along the applied force. The 2D representation of the tensegrity mechanism shown in Fig. 5b will be used for calculations. The force vectors on Fig. 5b can be calculated by the equation:

$$\mathbf{f}_i = \lambda_i \frac{\mathbf{d}_i}{\|\mathbf{d}_i\|} \qquad \text{with} \quad i = 1, 2, 3 \tag{6}$$

$$\text{where} \quad \mathbf{d}_i = \mathbf{b}_i - \mathbf{c}_i \quad \& \quad \mathbf{f}_i = [f_{ix}, f_{iy}, f_{iz}]^T$$

In Eqn. (6), λ_i represents the magnitude of applied forces. About the origin or central point A, there exist moments that are generated by the cables ($\mathbf{m}_c$) as well as the springs ($\mathbf{m}_s$) whose equations are given by:

$$\mathbf{m}_c = \sum_{i=1}^{3} (\mathbf{c}_i \times \mathbf{f}_i) \tag{7}$$

$$\mathbf{m}_s = \sum_{i=1}^{3} (k\ \mathbf{c}_i \times \mathbf{d}_i) \tag{8}$$

where k represents the stiffness of spring. We assume same stiffness for the three springs. The resultant moment $\mathbf{m}$ can be found by summing up the results of Eqn. (7) & Eqn. (8). For attaining stable postures, the sum of components

in the resultant moment $\mathbf{m}$ is equal to zero. As an example, if we assume $h = 1$, $\gamma = 1$, $k = 0.2$ N/mm, $\theta = 0$ radians and $\lambda_2 = \lambda_3 = 0$, the values of λ_1 could be estimated with respect to α. The equation of λ_1 is generated using Maple and it is given by:

$$\lambda_{1\ (\theta=0,\beta=\pi/2)} = \frac{-33 s_\alpha \sqrt{1 - s_\alpha}}{10 c_\alpha} \tag{9}$$

A tilt of α= 0 to $\pi/3$ radians is applied on the mechanism. For $\beta = 0$, the first cable cannot produce any moment to rotate around the y axis. Only the other cables can be used. For $\beta = \pi/2$, from Eqn. (9), it could be observed that the efforts generated have negative values and the mechanism tilts along the opposite direction of applied forces which is represented in Fig. 7.

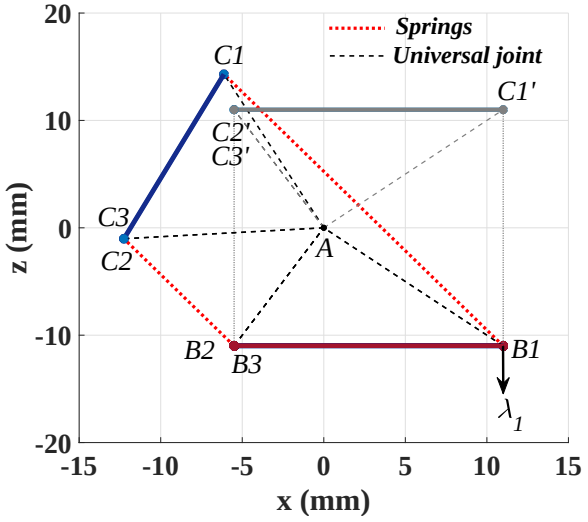

Figure 7: Representation of mechanism with applied force λ_1 along $C_1 - B_1$ with $\alpha = 0$ to $\pi/3$ radians and $\beta = \pi/2$ radians

The home-pose position of end-effector is represented in gray lines and points $C1' - C2' - C3'$ in Fig. 7. The final position is represented by $C1 - C2 - C3$. Thus, in order to have $m = 0$, preloading forces have to be applied which will ensure the stability of the mechanism.

Estimation of tilt limits

The feasible tilt range for the tensegrity mechanism has to be calculated. In Eqn. (4), the parameter γ in $\mathbf{o}_i$ can assume three values: $\gamma < 0$, $\gamma = 0$ and $\gamma > 0$. These are called as the Pendulum, the Neutral pose, and the Inverse-pendulum. We set $h = 1$ for this analysis. The estimation of tilt range also permits us to calculate the geometrical workspace of the mechanism. The tilt limits can be estimated by taking into account the articulation or joint limits of the mechanism. The equations of the robot and its associated constraint equations can be generated using the SIROPA[9, 10] package of Maple. By using the *CreateManipulator* syntax of SIROPA in Maple, the tensegrity mechanism is constructed. The tilt and azimuth angles are used as the pose variables and the lengths (l_1, l_2 and l_3) are employed as the articular variables. By using the *ConstraintEquations* of SIROPA, six constraint equations are generated, with first three equations at the lower limit of lengths and the next three equations at the upper limit of lengths. The equations are given by:

$$\mathcal{C}_{1+3i} : 2r_f^2 c_\alpha (c_\beta^2 - 1) - 2s_\beta s_\alpha r_f^2 (1+\gamma) + 2c_\alpha r_f^2 \gamma - 2r_f^2 c_\beta^2 + r_f^2 \gamma^2 + 3r_f^2 - l_j^2 \tag{10}$$

$$\mathcal{C}_{2+3i} : -2\sqrt{3} r_f^2 c_\alpha c_\beta s_\beta + 2\sqrt{3} r_f^2 s_\alpha c_\beta \gamma - 2c_\alpha c_\beta^2 r_f^2 + 2\sqrt{3} r_f^2 c_\beta s_\beta + 2\sqrt{3} r_f^2 c_\beta s_\alpha + 2s_\alpha s_\beta r_f^2 \gamma + 2r_f^2 c_\beta^2 + 2s_\alpha s_\beta r_f^2 + 4c_\alpha r_f^2 \gamma + 2r_f^2 \gamma^2 - r_f^2 c_\alpha + 3r_f^2 - 2l_j^2 \tag{11}$$

$$\mathcal{C}_{3+3i} : 2\sqrt{3} r_f^2 c_\alpha c_\beta s_\beta - 2\sqrt{3} r_f^2 s_\alpha c_\beta \gamma - 2c_\alpha c_\beta^2 r_f^2 - 2\sqrt{3} r_f^2 c_\beta s_\beta - 2\sqrt{3} r_f^2 c_\beta s_\alpha + 2s_\alpha s_\beta r_f^2 \gamma + 2r_f^2 c_\beta^2 + 2s_\alpha s_\beta r_f^2 + 4c_\alpha r_f^2 \gamma + 2r_f^2 \gamma^2 - r_f^2 c_\alpha + 3r_f^2 - 2l_j^2 \tag{12}$$

where for $i =$ 0 and 1, $l_j =$ l_{min} and l_{max}

These equations are generated using SIROPA by the projection of variables in a polynomial form [9]. For γ, three values are assumed $-1/4$, 0 and 1 and they are employed in Eqn. (10) to Eqn. (12). The value r_f is retained as 11 mm from existing prototype [5]. In order to estimate the geometric workspace range, the *CellDecompositionPlus* feature of the SIROPA package is employed. The *CellDecompositionPlus* uses the Cylindrical Algebraic Decomposition (CAD) technique and parametric root finding technique of Maple for estimating the regions where there exists real solutions to the inverse or direct kinematic problem [11]. For isolating the aspects around home-pose, we transform Eqn. (10) to Eqn. (12) as inequality equations [12] which will be used as inputs for *CellDecompositionPlus* in Maple. For the constraint equations, it is also necessary to set the length limits of l_i as it plays a vital role in the estimation of the maximum tilt angle. At the home-pose as represented in Fig. 5b, the length between $B - C$ is found to be 9 mm, 11 mm and 22 mm for γ= -1/4, 0 and 1. The constraint limits for these lengths under maximum tilt is assumed to be $l_{min} = 7$ mm and $l_{max} = 31$ mm for the analysis. The results of the geometric workspace are then generated for the three cases of γ and they are represented in Fig. 8.

It could be observed from the results that the maximum tilt range varies for the three case studies. The blue regions represents the feasible working range for the tensegrity mechanism. The values of tilt with azimuth angles at the joint limits are provided in Table 1.

Table 1: MAXIMUM TILT POSITIONS WITH AZIMUTH'S AT JOINT LIMITS

γ	β	α_{min}	β	α_{max}
-1/4		$-\pi/18$		$\pi/18$
0	[$\pm\pi/3$,$\pm\pi$]	$-\pi/6$	[$\pm 2\pi/3$, 0]	$\pi/6$
1		$-\pi/3$		$\pi/3$

From Table 1 and the results of Maple from Fig. 8, it can be deduced that the pendulum configuration is not ideal as the tilt range is narrow and cannot be feasible for pipes having angled or 90 degree bends. Better solutions are obtained in the other two cases but the inverse pendulum case is considered for further analysis as it could be potentially used for pipelines having bends up to 90 degrees as it has higher tilt ranges.

STATIC FORCE ANALYSIS OF THE MECHANISM

With the inverse pendulum configuration being a suitable solution for the tensegrity mechanism, it is important to analyze its stability. In the case of pipelines with junctions, the active compliance has to be employed where the stability of tensegrity mechanism could be controlled through cables and the robot can be made to follow the right direction. For passive compliance, the cable actuation is not required and the objective of the mechanism will be to overcome the bend under passive mode. In this scenario, the static stability of the mechanism has to be determined and it should be capable of working passively without cable actuation. As the suitable tilt and azimuth ranges have

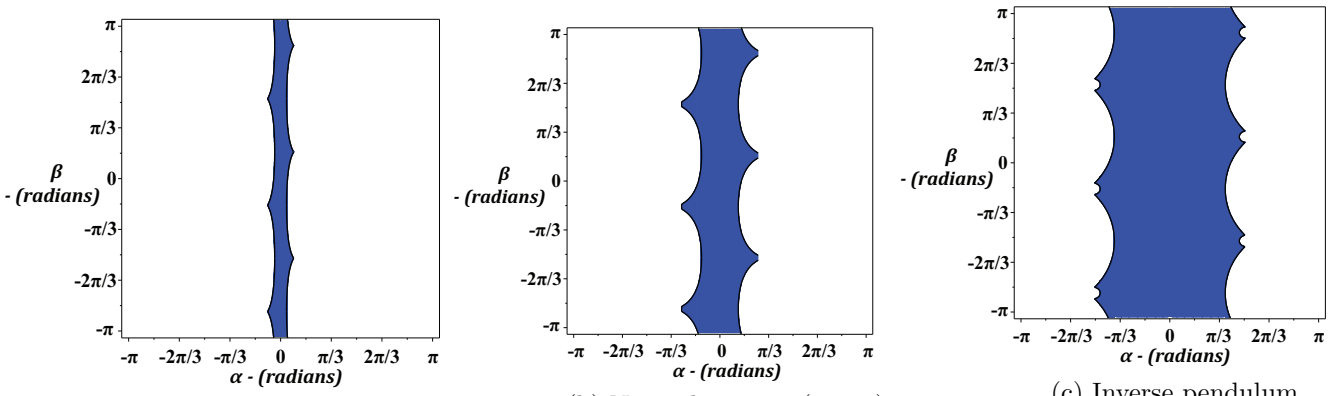

(a) Pendulum ($\gamma = -1/4$) (b) Neutral posture ($\gamma = 0$) (c) Inverse pendulum ($\gamma = 1$)

Figure 8: Geometric workspace range for the three case studies around the home-pose

been determined, the forces to be applied for the system can be estimated. According to Lagrange, for a moving system, the equation of motion [13] is given by:

$$\boldsymbol{\tau} = \frac{\mathrm{d}}{\mathrm{d}t}\left(\frac{\partial T}{\partial \dot{\mathbf{q}}}\right) - \frac{\partial T}{\partial \mathbf{q}} + \frac{\mathrm{d}U}{\mathrm{d}\mathbf{q}} \qquad \text{where} \quad \mathbf{q} = [\alpha, \beta]^T \tag{13}$$

where T and U are the kinetic and potential energies of the system. $\boldsymbol{\tau}$ represents the generalized torques on the system. Under static conditions, the velocity of the system is zero and there exists no kinetic energies. Thus in Eqn. (13) only the potential energy derivative with respect to the tilt and azimuth angles exists. The mass of the mechanism is also not taken into account as it vanishes along with the kinetic energy term. The potential energy of the system is contributed by the springs and cables. For this calculation, we assume the magnitudes of applied forces along the three cables as F_1, F_2, F_3 and equal stiffness for the three springs as k. The total potential energy can be estimated by summing up the energies of springs and cables. The equations are given by:

$$U_{cable} = \sum_{i=1}^{3} F_i l_i \quad U_{spring} = \sum_{i=1}^{3} \tfrac{1}{2} k l_i^2 \tag{14}$$

$$U_{tot} = U_{cable} + U_{spring} \tag{15}$$

The springs are considered massless and have zero free lengths. By substituting the results of Eqn. (15) in Eqn. (13), the forces required to actuate the mechanism can be calculated.

Stability of the tensegrity mechanism

Under zero-applied forces or under the presence of a preload, the mechanism can deform due to the springs. The stability of mechanism has to be analyzed under static modes. Arsenault et al. [14] analyzed that for a tensegrity mechanism to be stable under static modes, the second order derivative or the stiffness of the mechanism K has to be positive. The U_{tot} equation is first derived. Since the inverse pendulum configuration is used in the analysis, we fix γ = 1. U_{tot} depends on the applied forces as well as design parameters of the system and it can be expressed as:

$$U_{tot} = \sum_{i=1}^{3} f(F_i(\alpha, \beta, r_f, h)) + \zeta \tag{16}$$

where $\quad \zeta = 3\, k {r_f}^2 \left(\left(h^2 - \tfrac{1}{2}\right) c_\alpha + h^2 + \tfrac{1}{2}\right)$

At the home-pose condition as represented in Fig. 5b where we have α and β equal to zero and no applied forces, only the constant term ζ of Eqn. (16) exists as it depends on the spring stiffness k, mounting radius r_f, parameter h and the cosine of tilt. The stability of the system can be found by plotting the total potential energy against the estimated tilt ranges. The parameters k, r_f and h is considered as 0.2 N/mm, 11 mm and 1. The stability plot for the system is depicted in Fig. 9.

It could be observed that the mechanism remains unstable and has maximum potential energy with no forces being applied. Since U_{tot} has a direct dependency on the applied forces, the system continues to remain unstable when the preload is considered. Under the influence of zero applied forces, the mechanism has no dependencies on the azimuth

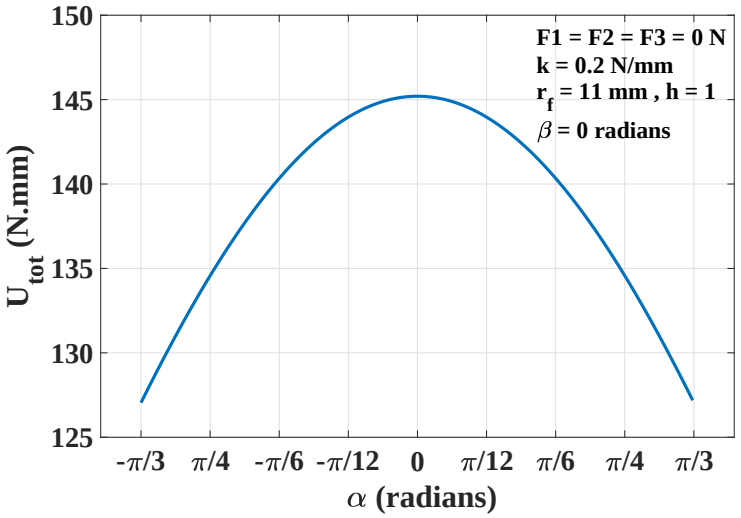

Figure 9: Plot of total potential energy versus the tilt with zero applied forces

angle (Eqn. (16)). The second order derivative of U_{tot} with respect to α which gives the mechanism stiffness K_α has to be studied for determining stable configuration [14]. The applied forces are considered equal and are taken as $F_1 = F_2 = F_3 = F$. The stiffness equation is generated using Maple with β & α at 0 radians and is given by:

$$K_\alpha = \frac{-3r_f\ \left(2\,k r_f\,h^2 + h\,F - k r_f\right)}{2} \tag{17}$$

It can be seen that the mechanism stiffness depends on the parameters r_f, h, F and k. By fixing one or several parameters, it is possible to determine a stable configuration. In this study, we fix the spring stiffness as per the prototype of Fig. 4 as 0.2 N/mm and a precharge of 2 N is considered for F. The stiffness K_α is then analyzed for varying values of h and r_f and their relations are shown in Fig. 10. As the parameter h increases towards 1, the

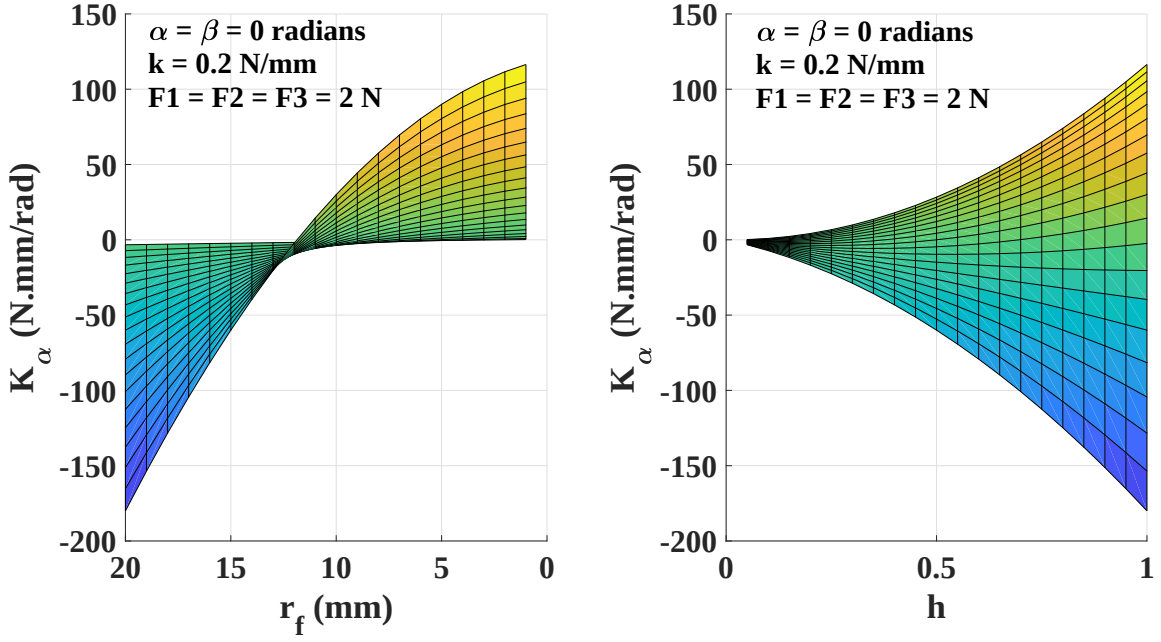

Figure 10: Projection of K_α with respect to r_f and h for α & $\beta = 0$ radians

positive zone of K_α is higher. However, K_α transforms into negative values when r_f increases. By retaining r_f as 11 mm from the existing design of the robot, a value of $h = 1/2$ is chosen such that stiffness K_α is always positive with the preload. The geometric workspace is calculated for this new inverse pendulum by using Eqn. (10) to Eqn. (12) and the results are depicted in Fig. 11. From the results of Fig. 11, it can be seen that the tilt range has been reduced

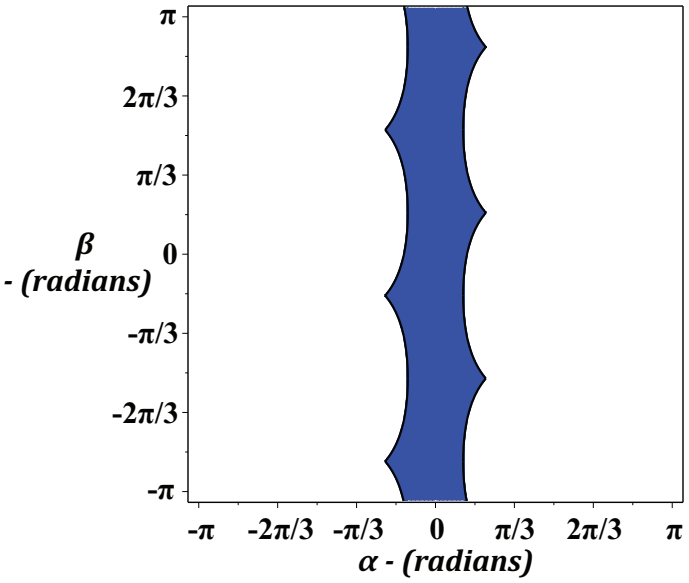

Figure 11: Geometric workspace for the new inverse pendulum configuration with h=1/2 and r_f = 11 mm

to $\pm$ $\pi/6$ radians. Using this range, the total potential energy is recalculated using Eqn. (16) for $\beta = 0$ radians and preload of 2 N. The result is depicted in Fig. 12. Even though the tilt limits have been reduced by almost half, a

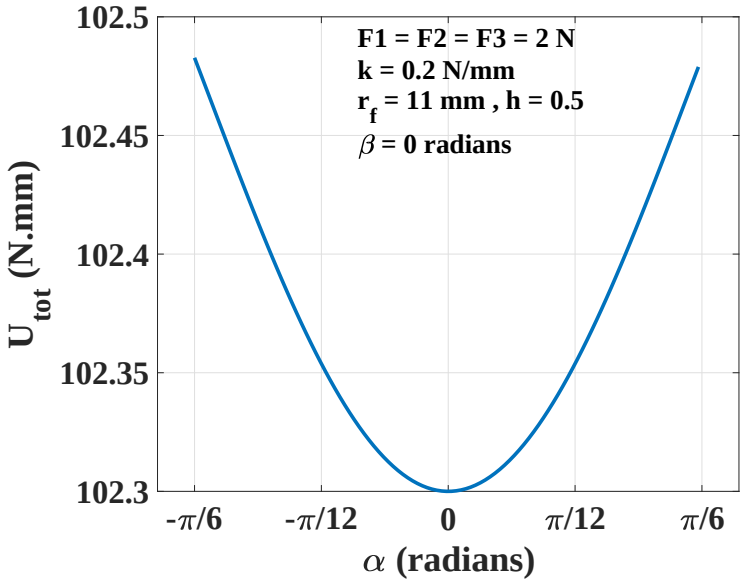

Figure 12: Plot of total potential energy versus tilt for new inverse pendulum configuration with preload of 2 N

stable configuration has been obtained. The system is also found to be stable with the consideration of preload. The new parameter of $h = 1/2$ will be considered for further analysis.

Estimation of forces to be applied and influences of azimuth β

In order to make the tensegrity mechanism to tilt upto a given angle, it is necessary to apply at least one force on the system. However, in order to obtain a given azimuth angle at a given tilt angle, at least two forces must be applied on the mechanism. The force equations can be solved by differentiating U_{tot} with respect to α & β and equating them to zero and fixing a positive value of 1 N.mm/rad for K_a. The forces can be expressed as:

$$F_i = f(\alpha, \beta, K_\alpha, h, r_f, k) \quad \text{with} \quad i = 1, 2, 3 \tag{18}$$

In Eqn. (18), the new inverse pendulum parameters identified in the previous section is considered. The azimuth angle β can vary from 0 to 2π radians and it can be controlled to attain a certain value based on the profile of pipeline

encountered by the robot. The three force values of Eqn. (18) are plotted against the azimuth range at the maximum tilt angle of $\pi/6$ radians which is depicted in Fig. 13.

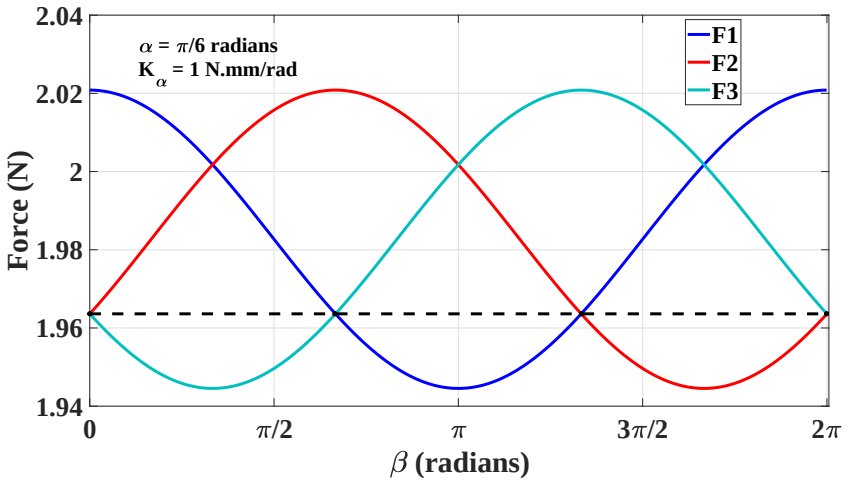

Figure 13: Variation of forces for $\beta = 0$ to 2π radians at $\alpha = \pi/6$ radians

In Fig. 13 for each azimuth phase of $2\pi/3$ radians one of the forces remain redundant. During the azimuth phase of 0 - $2\pi/3$, F_3 remains redundant and there exists no significant changes to the system by this force. On the other hand, the force F_1 continues to drop while F_2 starts increasing in this azimuth range. The dotted horizontal line in Fig. 13 separates the region of redundancy and below this line, one of the three forces always remain redundant. The influences of each azimuth phase on the three forces are provided in Table 2.

Table 2: INFLUENCES OF AZIMUTH PHASES ON THE FORCES

Azimuth (β) range	F_1	F_2	F_3
0 - $2\pi/3$	Decreasing	Increasing	Redundant
$2\pi/3$ - $4\pi/3$	Redundant	Decreasing	Increasing
$4\pi/3$ - 2π	Increasing	Redundant	Decreasing

However at azimuth angles of 0, $2\pi/3$ and $4\pi/3$ radians, the forces F_1, F_2 and F_3 are at a maximum while the other two forces will remain equal and low. Based on the profile of the pipeline, the cables used in the tensegrity mechanism could be actuated to attain an azimuth angle that will facilitate the robot to have better contact with the walls. For a curvilinear pipe profile in 3D space, at least one or maximum two forces have to be actuated while the third one always remains redundant.

CONCLUSIONS AND FUTURE WORKS

The tensegrity mechanism proposed in this article can be implemented as a solution to the rigid prototype of [4, 5] in order to work through pipelines with bends and junctions. By the study of compliances and tilt angle limits, the tensegrity mechanism was designed. For pipelines with 90 degrees bends, the universal joint can remain passive and it can address the issue of passive compliance. In the case of a junction, the cables can be actuated which will allow the robot to bend to a given tilt and azimuth to follow a given path. By correlating the tensegrity mechanism to a parallel manipulator, the orientation of mechanism was determined and the maximum tilt ranges were exploited by decomposition of the mechanism into three case studies. The inverse pendulum configuration was chosen as it provided the maximum tilt range. However, with the static force analysis, this system was found to be unstable under zero applied forces. By fixing several parameters, the parameter h was modified to obtain a stable configuration under the presence of preload. The variation of azimuth β on the mechanism was studied in order to determine the necessary forces to be applied while working through curved pipe profiles.

With the modification of h, the maximum tilt range was reduced from $\pm\pi/3$ to $\pm\pi/6$ radians . This range might not be sufficient to pass through a pipe bend of 90 degrees. This could be overcome by stacking a second tensegrity module over the existing mechanism. Kinematics and workspace analysis was performed by Furet et al.[15, 16] on stacked tensegrity system for 2D case. This problem will be extended for the 3D case because a stacked model can

provide higher tilt angles. Also with stacked modules, it will be essential to check stability as there will be two tilt angles. In this case, the Hessian matrix will be derived and stability can be attained when the determinant of the Hessian matrix is always positive. The CATIA model of the robot with stacked tensegrity modules that resembles an "Elephant Trunk" is depicted in Fig. 14. Force analysis will further be extended on the stacked models assembled with the robot for various postures inside pipeline namely: vertical, horizontal and angled configurations for understanding the stability of the entire robot. An alternate approach will be proposed which deals with the study of variation of spring stiffness k and its impact on the mechanism stiffness K_α. An optimization technique will also be carried out for the determination of spring stiffness by taking into account the general design equations of a tension spring.

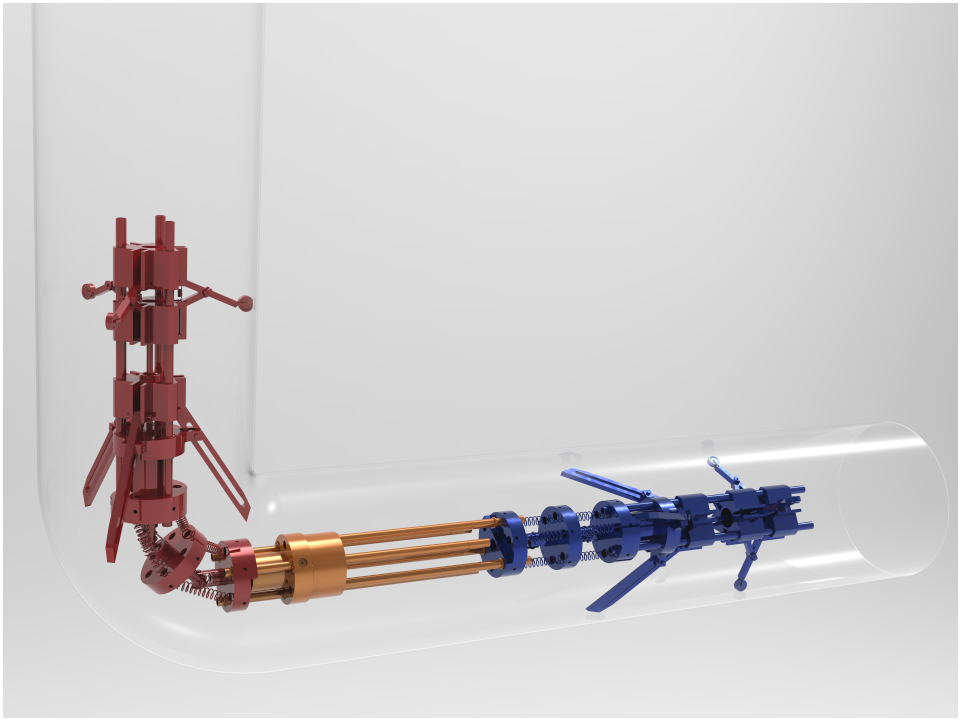

Figure 14: Modified architecture of the robot with stacked tensegrity structures in CATIA

References

[1] Nayak, A., and Pradhan, S., 2014. "Design of a new in-pipe inspection robot". *Procedia Engineering,* ***97***, pp. 2081–2091.

[2] Zhang, Y., Zhang, M., Sun, H., and Jia, Q., 2010. "Design and motion analysis of a flexible squirm pipe robot". In Intelligent System Design and Engineering Application (ISDEA), 2010 International Conference on, Vol. 1, IEEE, pp. 527–531.

[3] Kwon, Y.-S., Lim, H., Jung, E.-J., and Yi, B.-J., 2008. "Design and motion planning of a two-moduled indoor pipeline inspection robot". In Robotics and Automation, 2008. ICRA 2008. IEEE International Conference on, IEEE, pp. 3998–4004.

[4] Henry, R., Chablat, D., Porez, M., Boyer, F., and Kanaan, D., 2014. "Multi-objective design optimization of the leg mechanism for a piping inspection robot". In ASME 2014 International Design Engineering Technical Conferences and Computers and Information in Engineering Conference, American Society of Mechanical Engineers, pp. V05AT08A001–V05AT08A001.

[5] Chablat, D., Venkateswaran, S., and Boyer, F., 2018. "Mechanical design optimization of a piping inspection robot". In 28th CIRP Design conference.

[6] Yigit, C. B., and Boyraz, P., 2017. "Design and modelling of a cable-driven parallel-series hybrid variable stiffness joint mechanism for robotics". *Mechanical Sciences,* ***8***(1), pp. 65–77.

[7] Alici, G., and Shirinzadeh, B., 2004. "Topology optimisation and singularity analysis of a 3-sps parallel manipulator with a passive constraining spherical joint". *Mechanism and Machine Theory,* ***39***(2), pp. 215–235.

[8] Bonev, I., Zlatanov, D., and Gosselin, C., 2002. "Advantages of the modified euler angles in the design and control of pkms". In 2002 Parallel Kinematic Machines International Conference, Citeseer, pp. 171–188.

[9] Jha, R., Chablat, D., Baron, L., Rouillier, F., and Moroz, G., 2018. "Workspace, joint space and singularities of a family of delta-like robot". *Mechanism and Machine Theory*.

[10] Moroz, G., Chablat, D., Wenger, P., and Rouiller, F., 2010. "Cusp points in the parameter space of rpr-2prr parallel manipulators". In *New Trends in Mechanism Science*. Springer, pp. 29–37.

[11] Chablat, D., Ottaviano, E., and Moroz, G., 2011. "A comparative study of 4-cable planar manipulators based on cylindrical algebraic decomposition". In ASME 2011 International Design Engineering Technical Conferences and Computers and Information in Engineering Conference, American Society of Mechanical Engineers, pp. 1253–1262.

[12] Chablat, D., and Wenger, P., 1998. "Working modes and aspects in fully parallel manipulators". In Proceedings. 1998 IEEE International Conference on Robotics and Automation (Cat. No. 98CH36146), Vol. 3, IEEE, pp. 1964–1969.

[13] Meirovitch, L., 2010. *Fundamentals of vibrations*. Waveland Press.

[14] Arsenault, M., and Gosselin, C. M., 2006. "Kinematic, static and dynamic analysis of a planar 2-dof tensegrity mechanism". *Mechanism and Machine Theory,* ***41***(9), pp. 1072–1089.

[15] Furet, M., and Wenger, P., 2018. "Workspace and cuspidality analysis of a 2-x planar manipulator". In IFToMM Symposium on Mechanism Design for Robotics, Springer, pp. 110–117.

[16] Furet, M., Lettl, M., and Wenger, P., 2018. "Kinematic analysis of planar tensegrity 2-x manipulators". In International Symposium on Advances in Robot Kinematics, Springer, pp. 153–160.

NOMENCLATURE

Symbol	Description
α	Tilt angle of the tensegrity mechanism
β	Azimuth angle of the tensegrity mechanism
θ	Rotation of tensegrity mechanism about z-axis
$\mathbf{R}$	Resultant Tilt-Azimuth matrix
$\mathbf{b}_i$	Vector coordinates for base B_i
$\mathbf{c}_i$	Vector coordinates for end-effector C_i
l_i	Length of spring i
r_f	Radius of spring mounting points from flange centre
h	Scalar to determine position of base from origin
k	Stiffness of spring
γ	Scalar to determine end-effector position from origin
$\mathbf{f}_i$	Force vector
$\mathbf{m}_c$	Moment vector of forces caused by cables
$\mathbf{m}_s$	Moment vector of forces caused by springs
λ_i	Magnitude of cable forces
$\mathcal{C}$	Joint limits constraints
U	Potential energy of the system
F_i	Magnitude of applied forces through cables
K_α	Mechanism stiffness with respect to tilt α